SAND2019-7935C

Performance of a Tiled Array Compressive Sensing Spectrometer

Eric A. Shields

Sandia National Laboratories, 1515 Eubank Blvd SE, Albuquerque, NM U.S.A

ABSTRACT

A Compressive Sensing Snapshot Imaging Spectrometer (CSSIS) and its performance are described. The number of spectral bins recorded in a traditional tiled array spectrometer is limited to the number of filters. By properly designing the filters and leveraging compressive sensing techniques, more spectral bins can be reconstructed. Simulation results indicate that closely-spaced spectral sources that are not resolved with a traditional spectrometer can be resolved with the CSSIS. The nature of the filters used in the CSSIS enable higher signal-to-noise ratios in measured signals. The filters are spectrally broad relative to narrow-line filters used in traditional systems, and hence more light reaches the imaging sensor. This enables the CSSIS to outperform a traditional system in a classification task in the presence of noise. Lastly, simulation results on performing classification in the compressive domain will be shown. This obviates the need for the computationally-intensive spectral reconstruction algorithm.

Keywords: Compressive sensing, machine learning, imaging spectrometry

1. COMPRESSIVE SENSING SNAPSHOT IMAGING SPECTROMETER

Compressive sensing techniques have application to a wide range of imaging modalities, including spectrometry. Whereas in the last chapter we considered the case of imaging, in this chapter we investigate the use of compressive sensing for spectrometry and imaging spectrometry.

Previous work demonstrated that a single liquid crystal retarder could be used in conjunction with a point detector to create a compressive sensing spectrometer.[1] They measured 1024 spectral bands by making only 108 measurements. Their measurements were made by temporally varying the voltage across the liquid crystal cell. This approach was extended to an imaging geometry using both liquid crystals[2] and Fabry-Perot etalons.[3] These researchers also studied the performance of this system on spectral detection tasks.[4]

The approach used in these systems requires changing the system response temporally and hence does not directly translate to a snapshot spectrometer (i.e., a device capable of measuring spectral information in a single data collect). However, if the spectral filter system were spatially tiled with a small number of cells and each cell were to have a different voltage, a Bayer-filter-like sensor could be created. A Bayer-filter, shown in Figure 1, is the type of spectral filter used in the vast majority of digital cameras. It consists of a 2x2 tiling of red, green, and blue spectral filters (generally two green filters are used). Spatial resolution is traded for spectral capability. With a traditional Bayer filter 4 measurements are used to obtain 3 spectral bins. In a traditional spectrometer M measurements results in M spectral bins; with compressive sensing we aspire to obtain $N > M$ spectral bins.

The trade-off with a Bayer filter geometry is that spectral resolution is obtained at the expense of reduced spatial resolution. The spatial resolution of the system is governed by the size of the super-pixels rather than the individual pixels.

This tiled geometry is shown in Figure 2. This geometry is referred to here as the Compressive Sensing Snapshot Imaging Spectrometer (CSSIS). Broadband light is incident on an array of fixed spectral filters. In this figure a 4x4 geometry is shown, corresponding to 16 measurements. This 4x4 pattern defines a super-pixel and the pattern repeats across the entire detector array. In this chapter a "pixel" corresponds to the pattern seen by a single filter element. A "super-pixel" corresponds to a block containing a complete set of spectral filters.

Further author information: (Send correspondence to E.A.S.)
E.A.S.: E-mail: eashiel@sandia.gov, Telephone: 1 505 284 1984

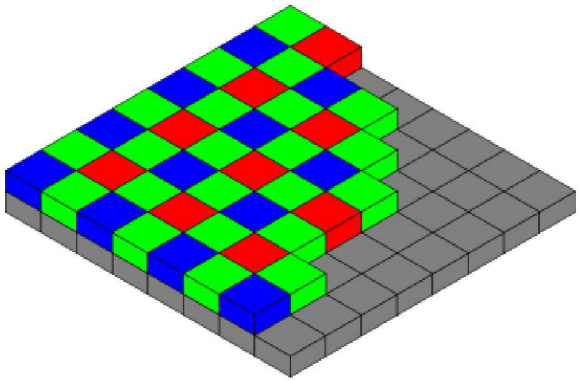

Figure 1. Traditional Bayer Filter Geometry

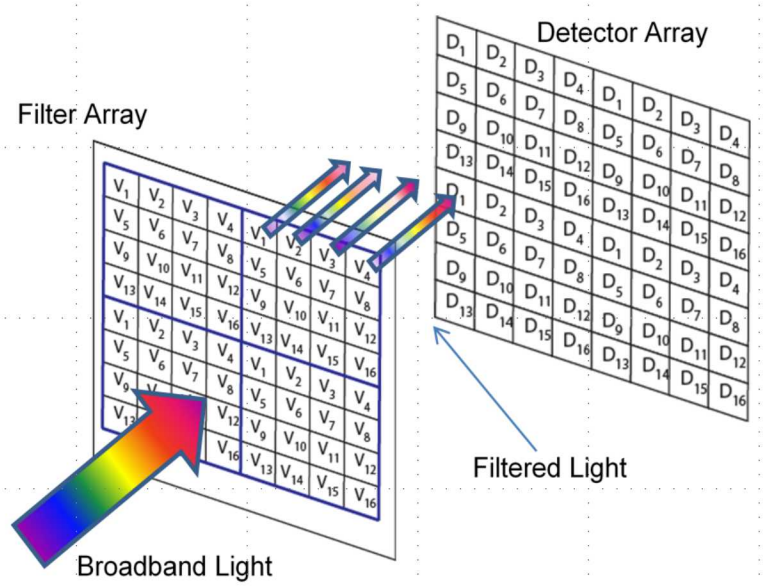

Figure 2. CSSIS Geometry

The spectral filters need not be liquid crystal filters. They can also be Fabry-Perot filters,[3] form birefringence filters, nano-antenna array filters, or any other type of device which can vary its transmittance (or reflectance) as a function of wavelength. This geometry has been implemented with dielectric filter stacks and studied by Kim, *et al.*[5]

This approach has several benefits. First, it is a true snapshot spectrometer; spectra are captured at the sample rate of the detector. This allows for spectral analysis of fast transient events. Furthermore, no temporal scanning or physical motion is required. Next, the system optical throughput is high. A traditional tiled spectrometer system employs narrow-band spectral filters that reject most of the light, leaving relatively little to be detected. The average transmittance of each filter in the CSSIS is much higher, perhaps 50%. Radiometric efficiency is significantly increased as much more light strikes the detectors. Lastly, since compressive sensing techniques can be used, the number of spectral bins is greater.

1.1 CSSIS Trade Space

The traditional tiled-spectrometer geometry is used for a variety of commercial applications. Commercial devices with array sizes of 4x4 and 5x5 are available.[6] Employing compressive sensing techniques dramatically changes the trade space in designing such systems.

1.1.1 Improved Spectral Resolution with Constant Spatial Resolution

One way this system could be leveraged is to provide increased spectral resolution while maintaining a constant spatial resolution. Consider replacing a 4x4 traditional filter array from an existing commercial system with a 4x4 compressive sensing filter array. Both of these systems have degraded the resolution of the imaging system by 4X since a 4x4 grid is used.

The traditional system uses its 4x4 filter array to obtain 16 spectral bins. However, the compressive sensing system could potentially use its 4x4 filter array to obtain 80 spectral bins. Thus the spectral resolution has been increased by 5X while maintaining the same spatial resolution.

1.1.2 Improved Spatial Resolution with Constant Spectral Resolution

The compressive sensing architecture could also be used to increase area coverage while maintaining spectral resolution. Consider replacing a 5x5 traditional filter array from an existing commercial system with a 3x3 compressive sensing filter array. The traditional system has degraded the resolution by 5X while the compressive sensing system has degraded the resolution by only 3X.

The traditional system obtains 25 spectral bins from its 25 spectral filters. The compressive sensing system could likewise obtain 25 spectral bins from its 9 spectral filters. Thus the spatial resolution of the compressive sensing system is better while the spectral resolution is the same.

1.1.3 Improved Area Coverage with Constant Spectral and Spatial Resolutions

Consider extending the previous example of a 5x5 traditional filter array and a 3x3 compressive sensing filter array. The compressive sensing system could be flown at a higher altitude so that its spatial resolution matches that of the traditional system. By flying the compressive sensing system 60% higher than the traditional system, the resolutions of the two systems would match. However, the area coverage of the compressive sensing system would be 2.56X the area coverage of the traditional system. Hence the compressive sensing system could see more of the ground at one time.

1.2 Spectral Super-Resolution

First, a study to determine the ability to obtain more spectral bins than measurements was conducted. A geometry using a 7x7 array of Fabry-Perot spectral filters was assumed, yielding $M = 49$ measurements. All filters were assumed to have the same light incident upon them (i.e., no spatial variation). The wavelength regime considered was in the long-wave infrared (LWIR): 7.8 to 12.7 μm. The reflectance of the mirrors of the Fabry-Perot etalons were assumed to be 80%. The mirror separations were constrained to be in the range of 40 to 100 μm and were optimized to minimize the system matrix coherence when the Daubechies-8 wavelets

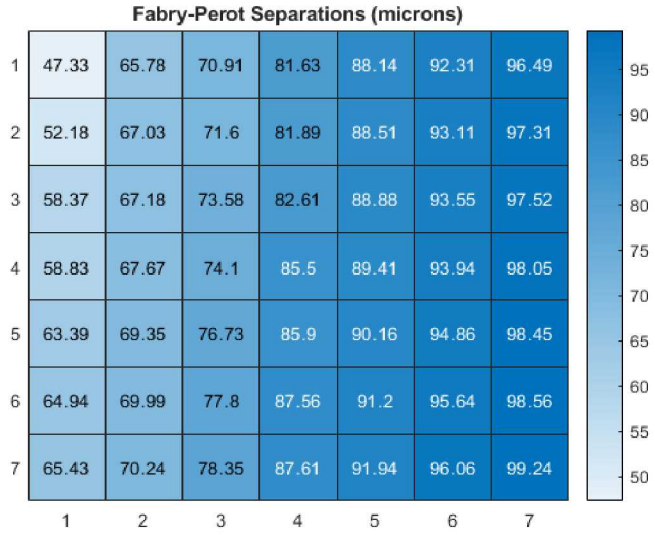

Figure 3. Fabry-Perot Filter Thicknesses

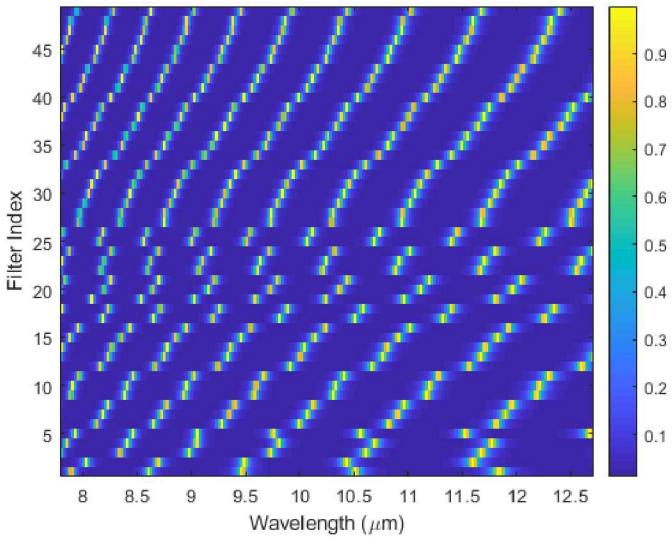

Figure 4. Super-Resolution Model Measurement Matrix

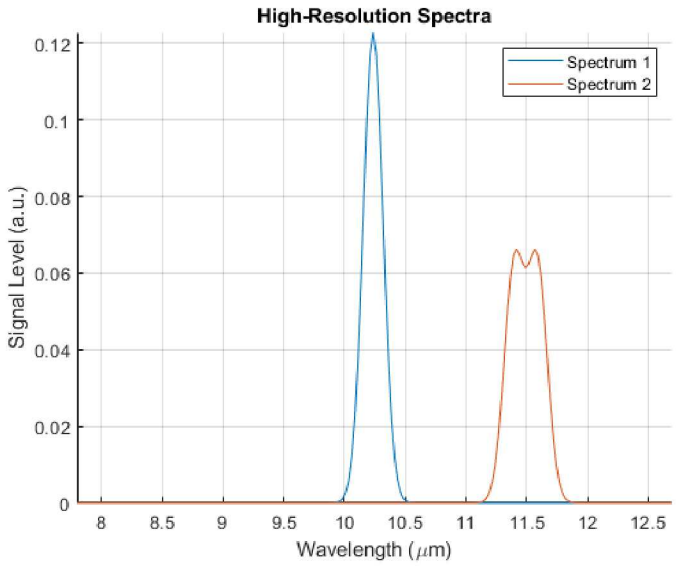

Figure 5. Spectra used for Spectral Super-Resolution Analysis

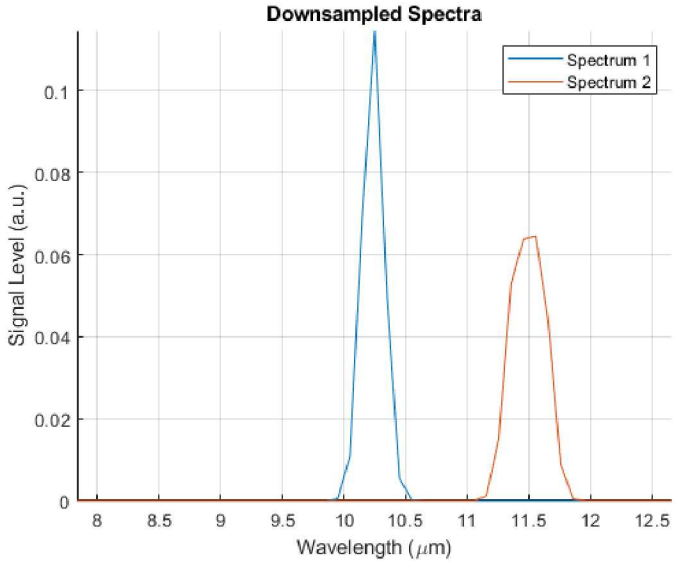

Figure 6. Downsampled Spectra

were used. Figure 3 shows the filter thicknesses and Figure 4 shows the spectral transmittances as a function of wavelength.

Two spectra were simulated. Spectrum 1 consists of a Gaussian centered at a wavelength of 10.24 μm with a full-width half-maximum (FWHM) of 0.191 μm. Spectrum 2 consists of a pair of Gaussians with the same FWHM of 0.191 μm but also separated by 0.191 μm centered about 11.49 μm. Both spectra were normalized to have unity energy. Figure 5 shows these two spectra sampled with $N = 196$ data points.

When these spectra are downsampled to 64 spectral bins, the spectral resolution is diminished such that the dip in Spectrum 2 is no longer resolved. Figure 6 shows the results of the downsampling operation.

Measurement with the CSSIS was simulated and the results are shown in Figure 7. Note that 64 measurements are made, the same number as in the downsampled case.

Reconstructions from the measurements shown in Figure 7 are shown in Figure 8. As can be seen from

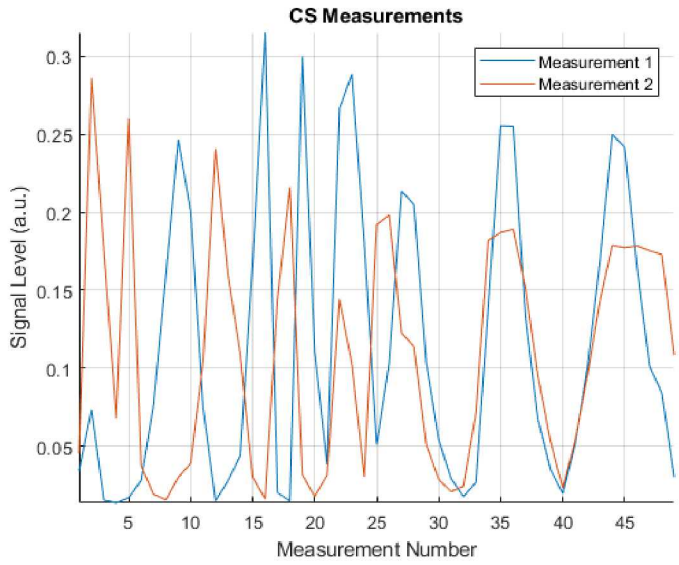

Figure 7. CSSIS Measurements of Spectra 1 and 2

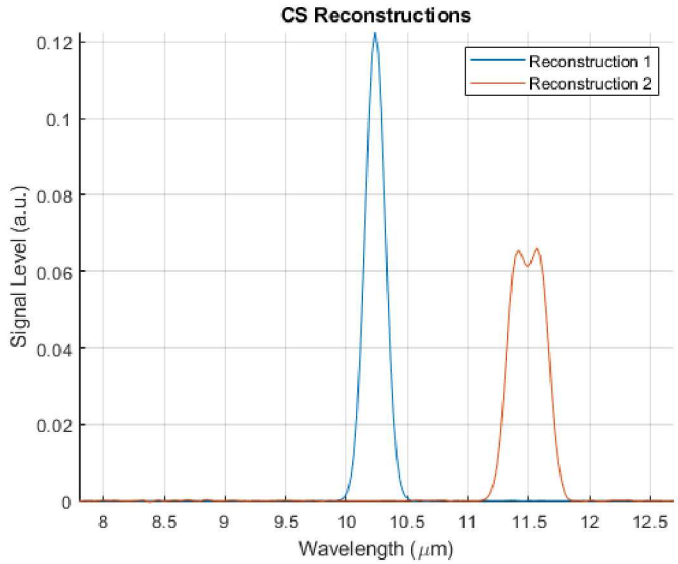

Figure 8. CSSIS Reconstructions of Spectra 1 and 2

this figure, the information about the dip is preserved. This indicates that more information is stored in the compressive sensing data than in the traditional spectrometer data.

Next, the impact of spatial variations was investigated. An optical imaging system with an f-number(defined as the ratio of the focal length to the aperture diameter) of 15 was used. The focal plane pixels were assumed to be 12 μm in size. The system point-spread function as a function of wavelength was modeled using standard Fourier optics theory. Figure 9 shows the PSF at a central wavelength at high spatial resolution. Figure 10 shows the PSF at a resolution of 12 μm, the size of an individual filter. Figure 11 shows the PSF at a resolution of 84 μm, the size of a super-pixel. The ensquared energy in a super-pixel ranges from 35.9% at the shortest wavelength to 16.5% at the longest wavelength.

A very simple spatial distribution of these two spectra was assumed. This distribution is shown in Figure 12. There is no variation in the Y-direction and a discontinuous change from Spectrum 1 to Spectrum 2 in the X-direction. These spatial distributions are convolved with the monochromatic point-spread functions to create

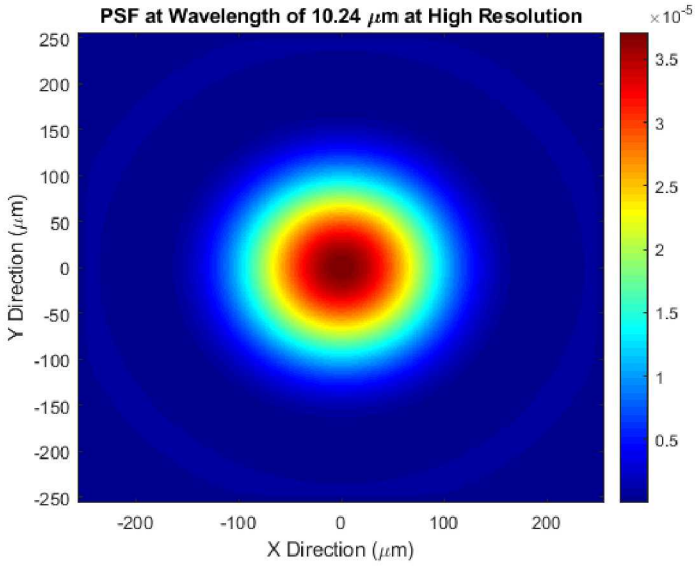

Figure 9. Point-Spread Function at 10.24 μm

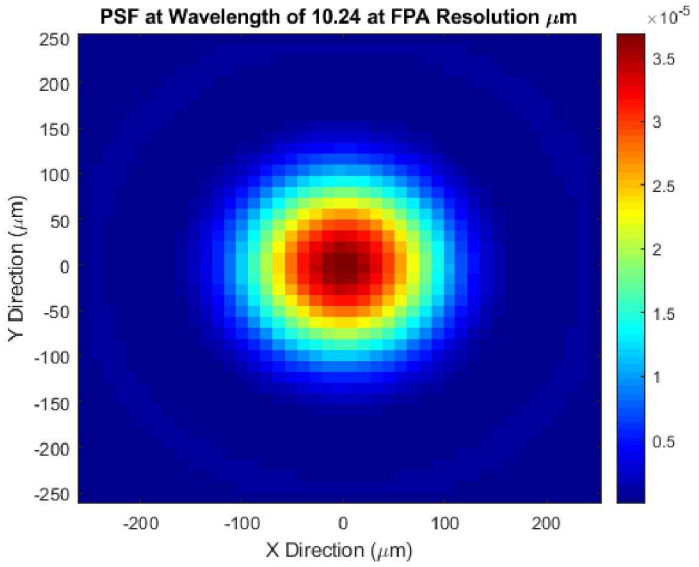

Figure 10. Point-Spread Function at 10.24 μm at Pixel Resolution

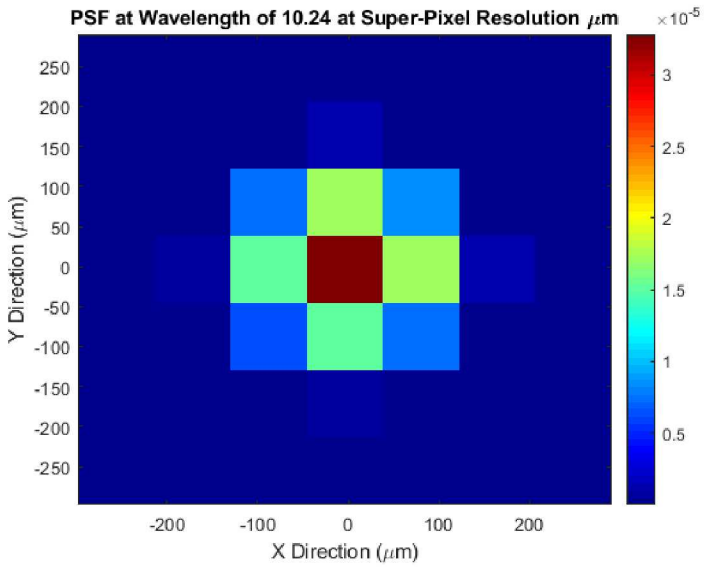

Figure 11. Point-Spread Function at 10.24 μm at Super-Pixel Resolution

spectral images at each wavelength. These spectral images are then sensed by the spectrometer.

Two spectrometers were simulated. The first is the CSSIS configuration described above. The second is a traditional spectrometer with 49 non-overlapping, perfect square-wave narrowband filters. The raw measurements from these systems are shown in Figures 13 and 14.

Spectral reconstructions shown across a slice in the X-direction are shown in Figures 15 and 16. Reconstructions in the Y-direction are not shown since there is no variation in the spectra in that dimension. These figures show that the CSSIS system is able to reconstruct the spectra accurately and that the effects of the spatial variation are localized to the spectral change boundary.

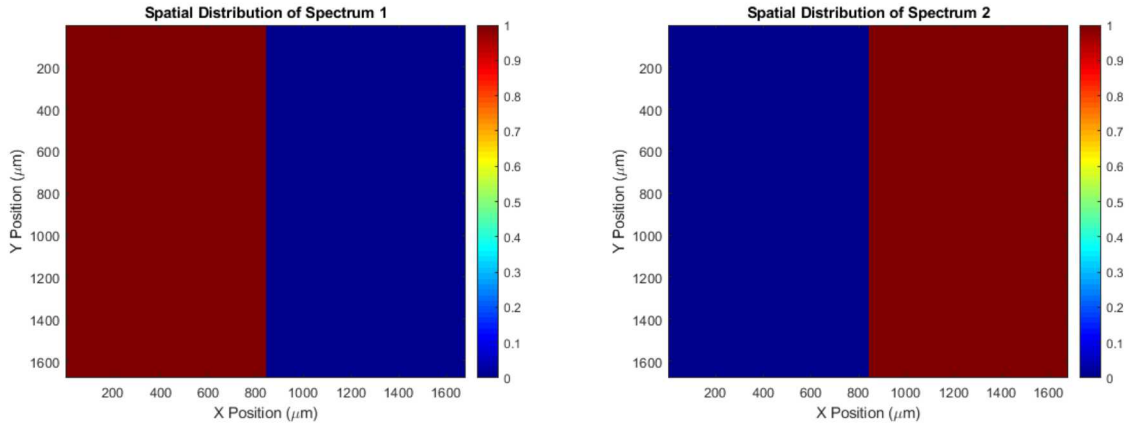

(a) Distribution of Spectrum 1 **(b)** Distribution of Spectrum 2

Figure 12. Spatial Distributions of Spectra 1 and 3

1.3 Spectral Classification

In the previous section we demonstrated that compressive sensing techniques can potentially store more information in the same number of measurements as compared to a traditional spectrometer system. In this section we explore how this impacts classification accuracy.

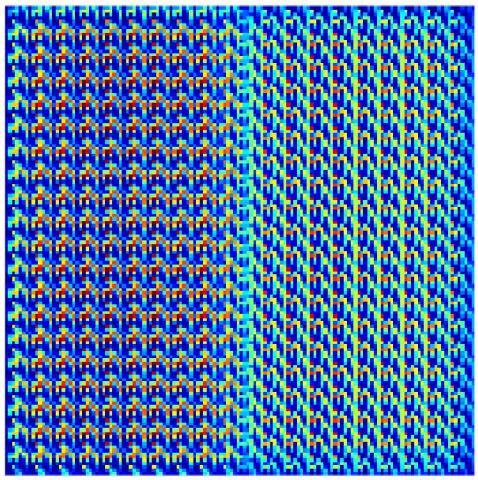

Figure 13. CSSIS Raw Image

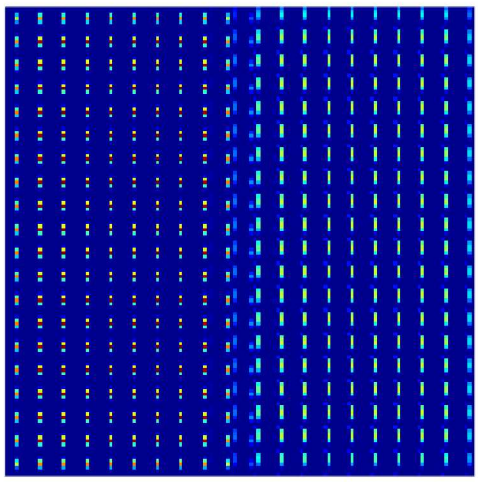

Figure 14. Traditional Spectrometer Raw Image

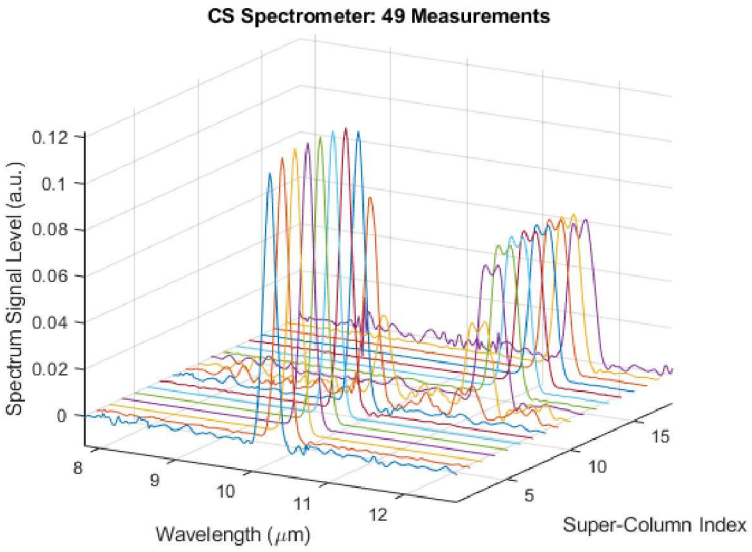

Figure 15. CSSIS Raw Image

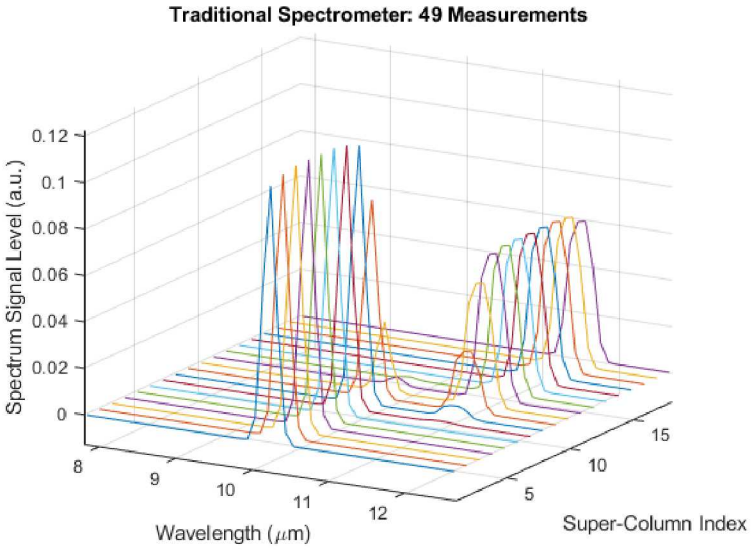

Figure 16. Traditional Spectrometer Raw Image

1.3.1 Averages of Indian Pines Classes

The Indian Pines data set is a hyperspectral image collected over the Purdue University agronomy farm in West Lafayette, Indiana.[7] The 145×145 image contains 220 spectral bands in the range 0.4 μm to 2.5 μm measured by the Airborne Visible/Infrared Imaging Spectrometer (AVIRIS). This data set includes ground truth data as well, making it useful for classification studies. This study investigated the ability of the CSSIS to distinguish between the averages of the 17 classes in this data set.

A different implementation of the CSSIS was used for this study. A 7x7 array of liquid crystal devices (LCDs) were used rather than Fabry-Perot spectral filters. The change in index of refraction of the LCD was varied between 0.001 and 1 in a linear fashion with an LCD thickness of 15 μm. Figure 17 shows the spectral transmittances of the filters. The Haar wavelet basis set was used.

For reconstructions, the ℓ_1-norm of the total variation (TV) of the wavelet coefficients was minimized rather than the ℓ_1-norm of the coefficients themselves. The total variation of a signal is the root-sum-square of the horizontal and vertical discrete gradients. Let $D_{h;i,j}(f)$ denote the horizontal discrete gradient of the signal f. Similarly let $D_{v;i,j}(f)$ denote the vertical discrete gradient f. We define $D_{h;i,j}(f)$ and $D_{v;i,j}(f)$ via

$$D_{h;i,j}(f) \begin{cases} f_{i+1,j} - f_{i,j} & i < n \\ 0 & i = n \end{cases} \tag{1}$$

and

$$D_{v;i,j}(f) \begin{cases} f_{i,j+1} - f_{i,j} & j < n \\ 0 & j = n \end{cases}. \tag{2}$$

The total variation is then defined via

$$TV(f) \equiv \sum_{i,j} \sqrt{(D_{h;i,j}(f))^2 + (D_{v;i,j}(f))^2}. \tag{3}$$

By minimizing the total variation of the wavelet coefficients, we force them to go to a constant value. Since we know the signal is sparse, this value is zero. This optimization technique worked better for this study than minimizing the ℓ_1-norm of the coefficients themselves.

A representative signal for each of the 17 classes in the Indian Pines data set was calculated by averaging all spectra assigned to that class. Figure 18 shows these spectra (blue lines) along with the CSSIS reconstructions (red lines). A compression factor of 4 was used, meaning that the 49 spectral measurements were used to produce 196 spectral bins.

Next, a classification study was conducted. The performance of the CSSIS system was compared with the performance of a traditional 7x7 tiled spectrometer array. In the traditional spectrometer the spectral filters were again considered to be ideal, non-overlapping square-wave filters with unity transmittance. The detector modeled for this analysis was assumed to have a 12-bit analog-to-digital converter (ADC) and full well depth corresponds to 100,000 electrons. A read noise of 4 electrons was assumed and the signals were nominally set to fill the well halfway. A Gaussian background noise was assumed to be present as well, with standard deviations of 0, 5, 10, 15, or 20 counts. For each class in the Indian Pines data set, 1,000 measurements were simulated. 70% of these were used for training purposes and 30% of these were used for testing purposes.

Classifications were performed on three different data sets. The first was the traditional spectrometer with 7x7 non-overlapping, ideal narrowband spectral filters. The second was the CSSIS raw data, consisting of 49 measurements through the CSSIS filters. The third was the CSSIS reconstruction into 196 spectral bins. In this case, the noise was added to the CSSIS data prior to reconstruction to simulate the physics of the device.

The classification algorithm was k-Nearest Neighbor classification where 5 nearest neighbors were used in the predictors. Figure 19 shows the results of these classifications. The classification accuracy is highest when

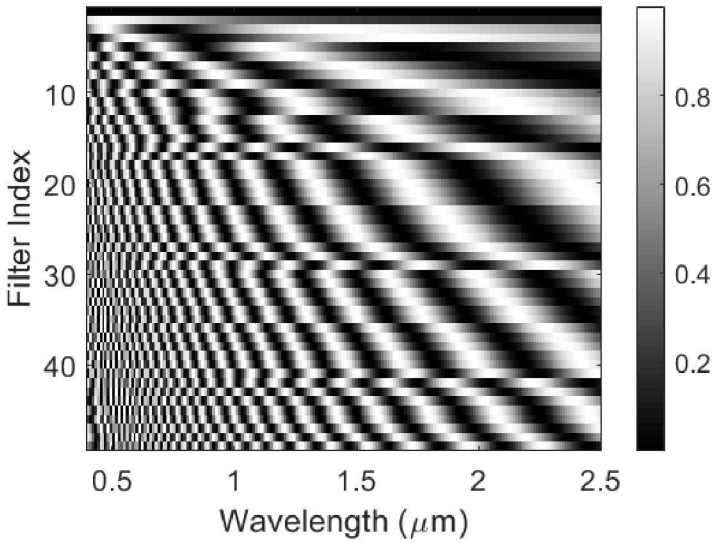

Figure 17. CSSIS Measurement Matrix for the Indian Pines Reconstruction Study

performed on the CSSIS raw data. Performing classification on the reconstructed data reduces the accuracy somewhat in the presence of noise. The traditional spectrometer performed the poorest.

One reason for the relatively poor performance of the traditional spectrometer in the presence of noise is the narrowband nature of the filters. The average transmittance across the spectral band for each filter is 1/49 = 2.04%. The average transmittance for the CSSIS spectral filters is roughly 50%. Therefore the CSSIS has a significant advantage in radiometric throughput over the traditional spectrometer. This is shown in Figure 20. In this case we define the signal-to-noise ratio (SNR) of the system as the mean of the spectral signal divided by its standard deviation. The CSSIS raw data has a significantly higher SNR in this sense that the traditional spectrometer or the CSSIS reconstruction.

The traditional spectrometer performance could likely be increased by increasing the integration time, but in that case the temporal performance of the spectrometer is reduced.

1.3.2 Indian Pines Data Set with Intraclass Variation

The previous study demonstrated that the CSSIS could distinguish between the classes in the Indian Pines data set. Intraclass variation was artificially induced via simulated read noise and Gaussian noise. Next, a study with the actual intraclass variation present within the Indian Pines data set was used.

The same CSSIS system as the previous section was used. The data used were the 145x145 spectral measurements in the Indian Pines data set. Ran *et al*, demonstrated that the Indian Pines data set can be effectively classified using a combination of an adaptive weighted filter (AWF) followed by a local Fisher discriminant analysis(LFDA) and K-nearest-neighbor (KNN) classification. That same approach was used here, with one small change. The AWF was modified to also include a Gaussian spatial weight distribution in the same manner as traditional bilateral filtering used for noise removal in digital images.[8] This filter is referred to as the bilateral adaptive weighted filter (BAWF). The filter employed used a windows size of 5 pixels and a spatial Gaussian distribution with a $1/e$-width of 2 pixels.

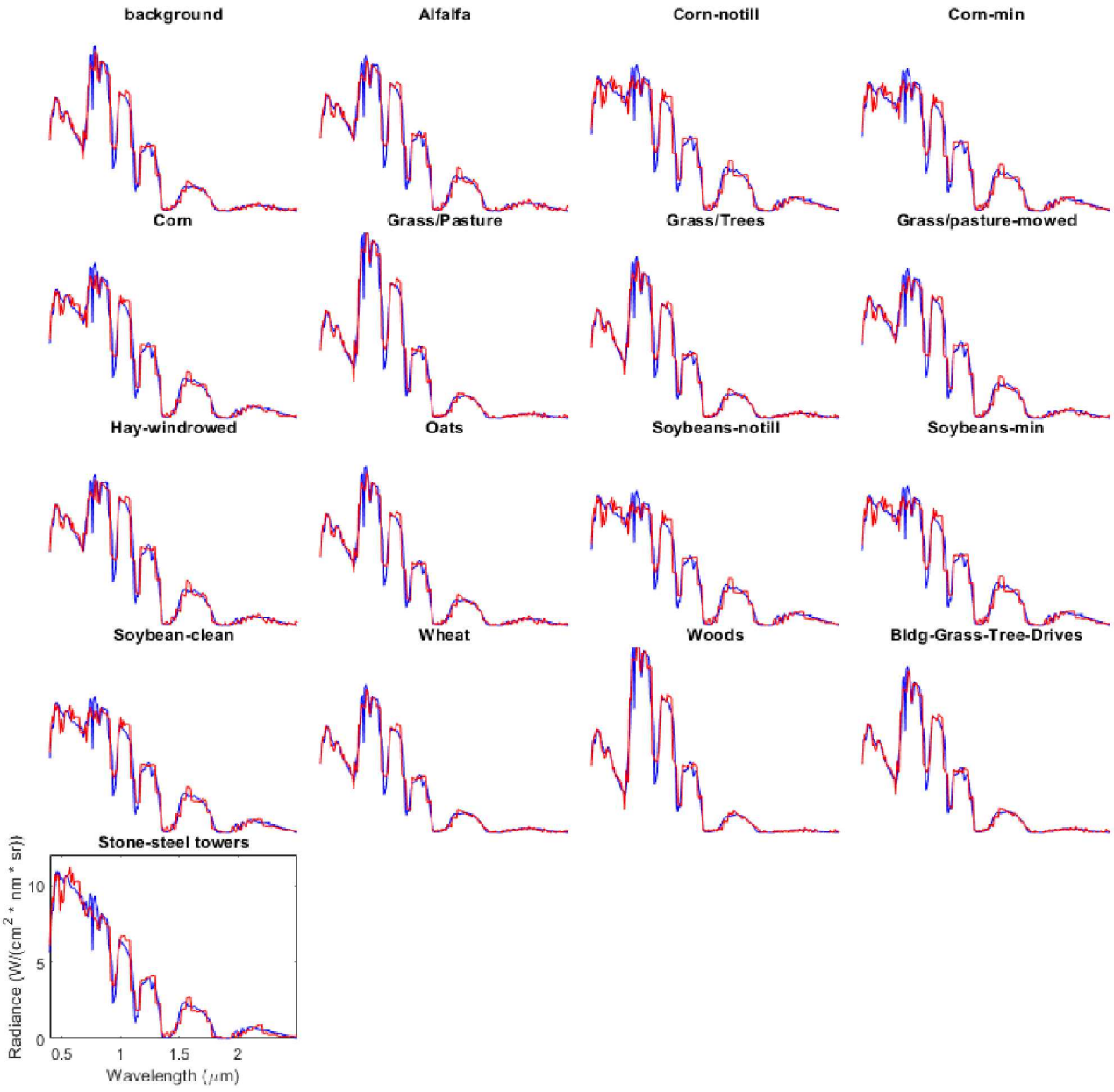

Figure 18. Indian Pines spectra (blue) and reconstructions (red) are shown. The last sub-plot shows the wavelength and radiance ranges used on all plots.

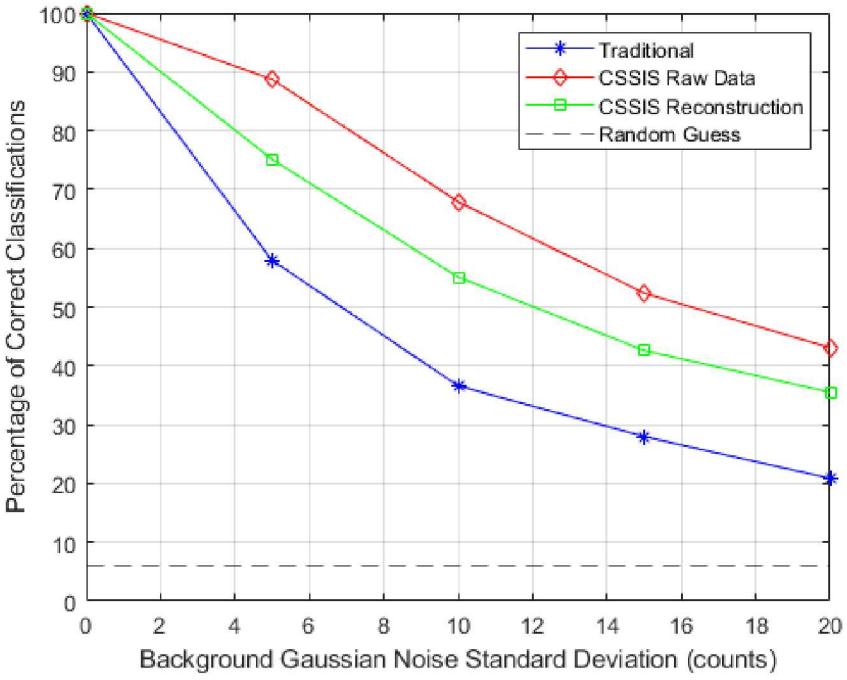

Figure 19. Classification Accuracy on Indian Pines Data Set

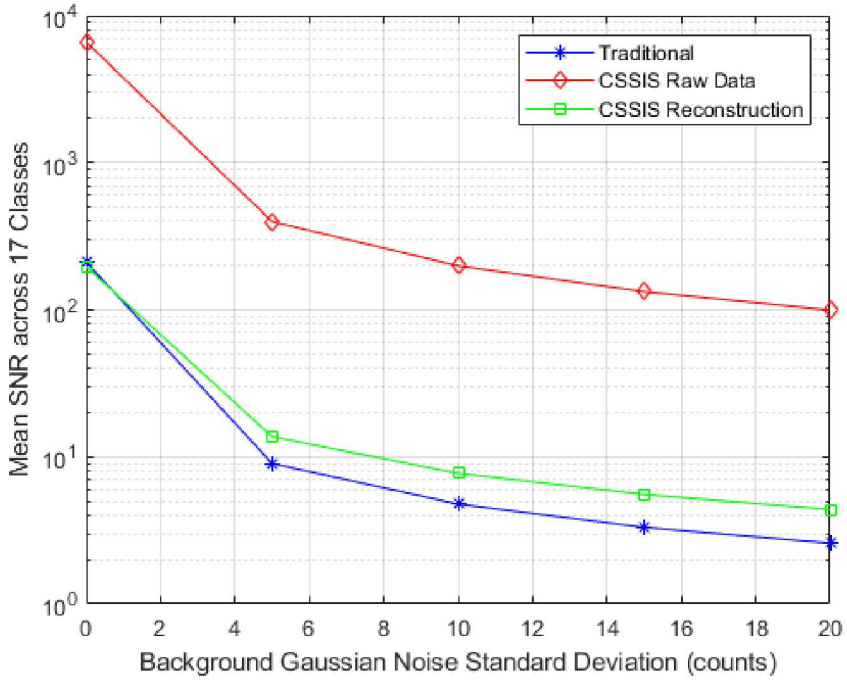

Figure 20. SNR of CSSIS and Traditional Spectrometer Signals

The Indian Pines data set were corrupted with noise in the same manner as previously described. 70% of the 145x145=21,025 pixels were used as the training set while the rest were used for testing. The following data sets were analyzed:

- Traditional: A traditional pixelated spectrometer using the BAWF-LFDA-KNN algorithm
- CSSIS Raw Data: The CSSIS spectrometer using the BAWF-LFDA-KNN algorithm on the raw CS data without reconstruction
- CSSIS Recon before Filtering: The CSSIS spectrometer where TV-reconstruction was performed and then followed with the BAWF-LFDA-KNN algorithm
- CSSIS Recon after Filtering: The CSSIS spectrometer where the BAWF algorithm was performed on the TV-recontructed spectra; LFDA-KNN were then performed on the reconstructed spectra.

Figure 21 shows the results

This study demonstrated that classification can be performed on the CSSIS raw data. In fact, the classification accuracy is higher for the CSSIS in the presence of noise as compared to an idealized traditional pixelated spectrometer.

Sandia National Laboratories is a multimission laboratory managed and operated by National Technology & Engineering Solutions of Sandia LLC, a wholly owned subsidiary of Honeywell International Inc., for the U.S.Department of Energy's National Nuclear Security Administration under contract DE-NA0003525.

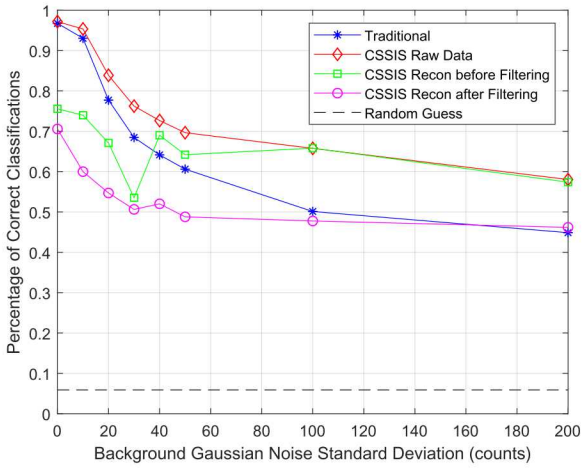

Figure 21. Classification Accuracy vs. Noise using the BAWF-LFDA-KNN Technique

ACKNOWLEDGMENTS

The author would like to acknowledge funding from Sandia's Laboratory Directed Research and Development program.

REFERENCES

[1] August, Y. and Stern, A., "Compressive sensing spectrometry based on liquid crystal devices," *Optics Letters* **38**(23), 4996–4999 (2013).

[2] August, I., Oiknine, Y., AbuLeil, M., Abdulhalim, I., and Stern, A., "Miniature compressive ultra-spectral imaging system utilizing a single liquid crystal phase retarder," *Scientific Reports* **6** (2016).

[3] Oiknine, Y., August, I., Blumberg, D. G., and Stern, A., "Compressive sensing resonator spectroscopy," *Optics Letters* **42**(1), 25–28 (2017).

[4] Gedalin, D., Oiknine, Y., August, I., Blumberg, D. G., Rotman, S. R., and Stern, A., "Performance of target detection algorithm in compressive sensing miniature ultraspectral imaging compressed sensing system," *Optical Engineering* **56**(4), 041312 1–6 (2017).

[5] Kim, C., Lee, W. B., Lee, S. K., Lee, Y. T., and Lee, H. N., "Fabrication of 2d thin-film filter-array for compressive sensing spectroscopy," *Optics and Lasers in Engineering* **115**, 53–58 (2019).

[6] Coffey, V. C., "Hyperspectral imaging for safety and security," *Optics & Photonics News* **26**, 26–33 (2015).

[7] Baumgardner, Marion F. Biehl, L. L. and Landgrebe, D. A., "220 band AVIRIS hyperspectral image data set: June 12, 1992 indian pine test site 3." https://purr.purdue.edu/publications/1947/1 (Sep 2015).

[8] Tomasi, C. and Manduchi, R., "Bilateral filtering for gray and color images," *Sixth International Conference on Computer Vision* , 839–846 (1998).